Numerical simulation and experimental validation of soil moisture infiltration patterns under underground porous membranes

Jinhong Shi[1,2,3], Xinlin He[1,2,3*], Yanwei Fan[4*], Chunxia Wang[1,2,3], Shuhan Chen[1,2,3]

(1. *College of Water Conservancy & Architectural Engineering, Shihezi University, Shihezi 832000, Xinjiang, China*;
2. *Key Laboratory of Cold and Arid Regions Eco-Hydraulic Engineering of Xinjiang Production & Construction Corps, Shihezi University, Shihezi 832000, Xinjiang, China*;
3. *National Center for Efficient Irrigation Engineering and Technology Research, Shihezi University, Shihezi 832000, Xinjiang, China*;
4. *School of Civil and Hydraulic Engineering, Lanzhou University of Technology, Lanzhou 730050, China*)

Abstract: In agricultural irrigation engineering, deep leakage is a key factor that significantly reduces the utilization efficiency of irrigation water. Underground installation of porous membranes, as a novel active regulation technology, can effectively reduce deep leakage losses of water in the soil through its physical barrier effect. However, the current understanding of the infiltration patterns of underground porous membranes remains inadequate, limiting the promotion and application of this technology. Therefore, this study integrates a methodology that combines numerical simulations with experimental validations. Using a non-membrane treatment as a control (CK), this study investigated the soil water infiltration of underground porous membranes under various combinations of saturated hydraulic conductivity (K_s), porous membrane diameter (D), burial depth (H), and spacing (S). The results indicated that under the four types of aeolian sandy soil conditions, underground installation of porous membranes had a significant impact on soil infiltration characteristics, exhibiting an infiltration-reducing effect. Upon entering the steady infiltration stage, the minimum reduction in the infiltration rate for the various porous membrane treatments was 2.86 times that of the CK treatment. At a specific irrigation time (t), the steady infiltration rate (i_f) and cumulative infiltration (I) of soil increased with increasing K_s, D, H, and S. There was a strong power function relationship between i_f and the four factors (R^2=0.997), with a coefficient of 0.209, and exponents of 1.14, 1.04, 0.48, and 0.30, respectively. Furthermore, based on the Kostiakov infiltration model and comprehensively considering K_s, D, H, S, and t, an estimation model for cumulative infiltration of underground porous membranes was developed. The reliability of the estimation model was assessed using experimental data, with the root mean square error approaching 0 and the Nash-Sutcliffe efficiency coefficient close to 1, indicating the good predictive performance of the model. The findings of this study can provide a scientific basis for the operation and management of underground porous membrane irrigation projects.

Keywords: underground porous membrane, steady infiltration rate, cumulative infiltration, estimation model, HYDRUS-2D/3D

DOI: 10.25165/j.ijabe.20251806.9886

Citation: Shi J H, He X L, Fan Y W, Wang C X, Chen S H. Numerical simulation and experimental validation of soil moisture infiltration patterns under underground porous membranes. Int J Agric & Biol Eng, 2025; 18(6): 144–157.

1 Introduction

In arid and semi-arid aeolian sandy areas, the combined effects of natural factors (such as water resource scarcity and poor soil quality) and human activities (including excessive cultivation and extensive irrigation) have led to increasingly severe land desertification issues[1,2]. This process is often accompanied by the degradation of the soil structure, which facilitates the formation of aeolian sandy soils characterized by strong permeability. Owing to their loose texture and poor water and nutrient retention, such soils result in significant deep leakage of both irrigation water and natural precipitation in agricultural fields, which severely restricts the efficient use of agricultural water resources[3,4]. Currently, regarding the status of agricultural irrigation, although existing water-saving irrigation technologies can effectively alleviate deep leakage, issues related to water-resource waste persist[5]. This is because current technical systems primarily focus on optimizing irrigation methods and regulating the spatial uniformity of moisture[6,7]. However, it remains predominantly passive in adapting to natural conditions, such as uneven rainfall, soil spatial heterogeneity, and dynamic soil moisture variations[8-10], and lacks active control measures. Therefore, the pursuit of deep leakage control methods that actively regulate soil water movement is of practical importance.

In recent years, soil anti-seepage technologies, such as straw deep burial, inter-layer soil placement, and underground film placement, have rapidly advanced. These technologies primarily demonstrate significant effects on soil improvement, moisture regulation, and crop yield enhancement through physical barriers or

Received date: 2025-04-30 **Accepted date:** 2025-09-13

Biographies: Jinhong Shi, PhD Candidate, research interest: water-saving irrigation, hydrology and water resources, Email: 1042214130@qq.com; **Chunxia Wang**, Associate Professor, research interest: theory and technology of water-saving irrigation, Email: 410443356@qq.com; **Shuhan Chen**, Master, research interest: hydrology and water resources, Email:1902896640@qq.com.

***Corresponding author: Xinlin He**, Professor, research interest: efficient utilization of water resources in arid areas. College of Water Conservancy & Architectural Engineering, Shihezi University, Shihezi, Xinjiang 832000, China. Tel: +86-15309934677, E-mail: hexinlin@shzu.edu.cn; **Yanwei Fan**, Associate Professor, research interest: numerical simulation of soil hydrodynamic processes. School of Civil and Hydraulic Engineering, Lanzhou University of Technology, Lanzhou 730050, China. Tel: +86-15095330393, Email: fanyanwei24@163.com.

biological regulation[11-13]. However, although straw deep burial can enhance the organic matter content of the soil, its slow decomposition in anaerobic environments can release substantial amounts of organic acids that may adversely affect root growth[14]. Although interlayer soil placement can impede water infiltration, its effectiveness is influenced by differences in water potential caused by varying water absorption capacities of the materials[15]. Furthermore, although films placed underground can effectively inhibit water leakage, completely sealed underground barriers hinder gas exchange in the soil. This lack of controllable drainage pathways can negatively affect farmland, resulting in excessively high moisture content in the root zone and consequently decreasing seedling survival rates[16]. Therefore, underground porous membrane technology (Figure 1) has garnered attention as an innovative method for moisture regulation. This technology involves embedding biodegradable polymer film materials beneath the tillage layer, typically 20-50 cm below the surface, and utilizing their unique porous structure to facilitate slow and uniform water infiltration into the soil. It has significant potential to enhance irrigation efficiency and reduce deep leakage[17]. Compared with traditional underground barrier technologies, the porous membrane system offers significant advantages: 1) it alters the conventional root-zone wetting pattern, resulting in a more uniform distribution of moisture in the surface layer and reducing deep leakage of irrigation water; 2) its porous structure facilitates controlled drainage, preventing water accumulation and hypoxia in the root zone, thereby providing a suitable growth environment for plants; and 3) the design of circular hole structures allows roots to penetrate vertically without affecting their development, achieving low maintenance and long-term use. Therefore, it is essential to conduct comprehensive research on the mechanisms by which underground porous membranes regulate soil moisture infiltration to reveal their universal patterns.

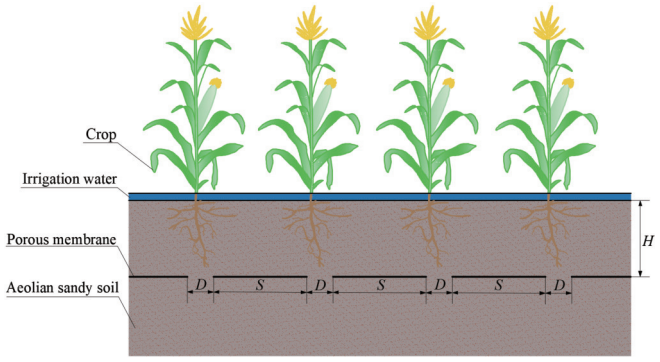

Note: D is porous membrane diameter; H is porous membrane burial depth; S is porous membrane spacing.

Figure 1 Schematic diagram of underground porous membrane

Currently, there are relatively few studies on underground porous membranes. Hong et al.[18] conducted pot experiments by placing membranes with different porosities at various depths within the root zone soil to investigate the impact of porous membrane placement on the soil moisture distribution. They found that when the membrane was positioned at a depth of 20 cm, the maximum soil moisture content occurred 5 cm below it. By monitoring changes in soil water storage at a depth of 30 cm, they discovered that the treatment with a laying depth of 15 cm and porosity of 50% reduced water consumption by 23.0% compared with the bare soil treatment, indicating that this technology was effective in conserving water. Based on this, Qin et al.[17,19] conducted indoor infiltration, evaporation, and pot experiments, and found that at a porosity of 30% and a burial depth of 15 cm, both the water infiltration rate and leakage amount were minimized. The cumulative evaporation from the surface of the soil treated with 40% porosity was reduced by 18.67% compared with the no-membrane treatment. Additionally, the plant physiological growth indicators increased with increasing burial depth. Specifically, stem diameter growth was enhanced at burial depths of 15 and 20 cm, and a burial depth of 20 cm also increased plant yield and water use efficiency, effectively demonstrating the benefits of this technology in reducing leakage, inhibiting evaporation, and conserving water, while increasing yield. These experimental studies enable precise control over various experimental variables and serve as fundamental methods for revealing the principles governing soil moisture movement. However, multifactor completely randomized experiments are time-consuming, labor-intensive, and challenging to control. With the rapid advancement of computer technology, numerical simulation methods are increasingly being used in the field of agricultural irrigation and have become an effective means of quantitatively analyzing the characteristics of soil moisture movement and its influencing factors. HYDRUS software, developed by Šimůnek et al.[20,21], has demonstrated strong adaptability and reliability in simulating soil moisture movement under various irrigation conditions. Based on this foundation, many researchers have used HYDRUS to conduct simulation studies on the transport characteristics of soil moisture under different irrigation scenarios. For instance, Fan et al.[22] used HYDRUS-2D to analyze the effects of various factors, including soil-saturated hydraulic conductivity, drip discharge, and tube parameters, on the movement of soil moisture in vertical tube surface drip irrigation scenarios. Based on the numerical simulation results, they developed a model to estimate steady soil infiltration rates and the transport of wetting fronts, which was validated using experimental methods. Sun et al.[23] used the HYDRUS-2D model to simulate and validate indoor experiments on canal leakage under layered sandy soil conditions. They examined the variations in cumulative and steady infiltration rates during the infiltration process at different water head levels, as well as the movement patterns of the wetting front of infiltrated water in the soil surrounding the channels. HYDRUS-2D/3D can be effectively used to characterize soil moisture movement under various irrigation scenarios. Previous studies on underground porous membranes have primarily used experimental methods. However, studies using the HYDRUS-2D/3D model to simulate the effects of various combinations of factors, including soil texture, membrane diameter, burial depth, and spacing on soil moisture movement, have not been reported. Therefore, to ensure the rational application of underground porous membrane technology, it is crucial to elucidate the infiltration patterns of soil under different influencing factors, as this is essential for effectively regulating soil moisture distribution.

This study used a combined approach of HYDRUS-2D/3D simulations and laboratory experiments to investigate the mechanisms by which underground porous membranes influence soil infiltration characteristics. In addition, the quantitative relationships between the membrane parameters, such as diameter, burial depth, and spacing, and the steady infiltration rate and cumulative infiltration amount of the soil were explored, ultimately establishing an estimation model. The objectives of this study were as follows: 1) to examine the soil moisture infiltration process under underground porous membrane technology, using a no-membrane treatment as a control, and to preliminarily assess the feasibility of

using underground membranes for water retention; 2) to conduct a comparative analysis of the effects of various parameters of underground porous membrane technology on soil infiltration rate and cumulative infiltration; and 3) to develop estimation models for steady infiltration rate and cumulative infiltration under underground porous membrane technology. This study aimed to clarify the impact of irrigation technical factors on soil infiltration characteristics under conditions of buried porous membranes to provide scientific evidence to support the widespread application of underground porous membrane technology in arid and semi-arid sandy regions.

2 Materials and methods

2.1 Experimental materials

Soil samples were collected from the Sand Plant Garden in Minqin County and Babusha Forest Farm in Gulang County, Gansu Province. The soil type was aeolian sandy soil with a sampling depth of 0-40 cm. Minqin aeolian sandy soil was used to verify the accuracy of the simulation results obtained from the HYDRUS-2D/3D software, whereas Gulang aeolian sandy soil was used to validate the reliability of the estimation model developed in this study. The collected experimental soil samples were air-dried, compacted, and mixed evenly before passing through a 2 mm sieve to prepare the indoor soil samples. The saturated water content and saturated hydraulic conductivity of the Minqin and Gulang aeolian sandy soils were measured through experimental methods. Soil bulk density was measured using the ring knife method, and the soil particle size distribution was determined using a laser particle size analyzer. The soil characteristic parameters are listed in Table 1. Other hydraulic characteristic parameters of the tested soils were inverted using the Rosetta module of the HYDRUS-2D/3D software, and they were corrected.

Table 1 Different experimental soil characteristic parameters

Soil type	Particle size mass fraction/%			Saturated water content/cm³·cm⁻³
	<0.002 mm	0.002-0.020 mm	0.020-2.000 mm	
Minqin aeolian sandy soil	95.32	3.58	1.10	0.434
Gulang aeolian sandy soil	92.92	4.62	2.46	0.345

2.2 Experimental equipment and methods

The experimental setup primarily consisted of an adjustable support frame, Mariotte bottle, rubber hose (outlet pipe), acrylic soil box, and biodegradable porous membrane (thickness: 2 mm, with pore diameters of 4, 6, 8, and 10 cm) (Figure 2). The Mariotte bottle, positioned on a stand, was marked with clear scale lines, had a diameter of 10 cm, and a height of 100 cm. To ensure the airtightness of the system, the connecting hose of the Mariotte bottle was secured to the inner wall of the soil box using a water stop clamp. The soil box was constructed from 10 mm acrylic plates, with all sides tightly bonded to prevent any water leakage. The dimensions of the boxes were 30 cm×30 cm×65 cm, 40 cm×40 cm×65 cm, 50 cm×50 cm×65 cm, and 60 cm×60 cm×65 cm (length×width×height). Additionally, a soil sampling hole was positioned on the side, and a ventilation hole (with a diameter of 2 mm) was located at the bottom to prevent air blockage, which could adversely affect the experimental results.

Before the experiment commenced, the prepared different soil samples were loaded into the soil boxes in layers (5 cm), following the experimental scheme outlined in Table 2. Specifically, the Minqin aeolian sandy soil and Gulang aeolian sandy soil were layered according to the prescribed dry bulk density of γ= 1.52 g/cm³. The interfaces between the layers were roughened to enhance the soil contact. Once the height of the filled soil reached the designated experimental depths of 25, 30, 35, and 40 cm, a porous membrane was placed, with one quarter of the membrane holes located at the corners of the soil box. During the experiment, a Mariotte bottle was used to maintain a constant water head for irrigation, and the readings from the Mariotte bottle were recorded at predetermined intervals. After the experiment, soil samples were collected from the sampling hole to determine the moisture content.

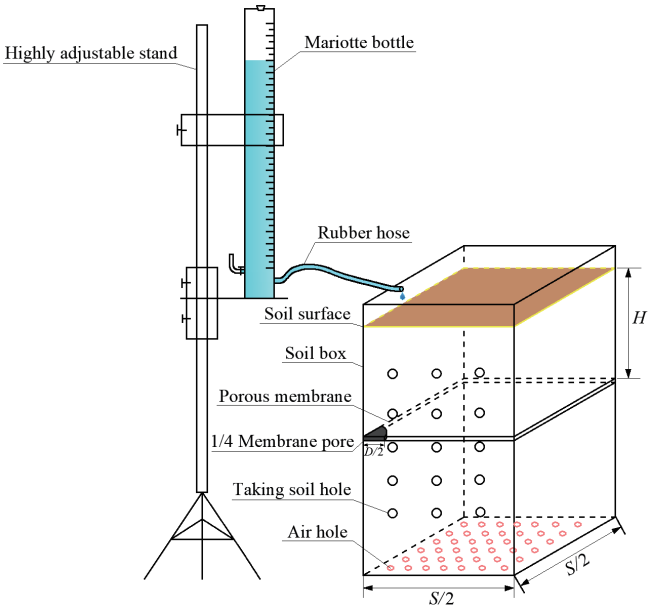

Note: $D/2$ is half the diameter of the porous membrane; H is porous membrane burial depth; $S/2$ is half of the porous membrane spacing.

Figure 2 Schematic diagram of the underground porous membrane infiltration test device

Table 2 Indoor experimental scheme under different aeolian sand conditions

Scheme number	Soil sample points	K_s/cm·min⁻¹	D/cm	H/cm	S/cm
1	Minqin	0.218	4	40	30
2	Minqin	0.218	6	35	50
3	Minqin	0.218	8	30	40
4	Minqin	0.218	10	40	60
5	Gulang	0.398	4	40	30
6	Gulang	0.398	6	35	50
7	Gulang	0.398	8	30	40
8	Gulang	0.398	10	25	40

Note: K_s denotes soil saturated hydraulic conductivity; D denotes porous membrane diameter; H denotes porous membrane burial depth; S denotes porous membrane spacing.

2.3 Mathematical models

2.3.1 Basic equation

Assuming that the soil is homogeneous and isotropic, the underground porous membrane can be conceptualized as an axisymmetric, two-dimensional infiltration process. The governing equation for soil moisture movement is the Richards equation, which is expressed as follows:

$$\frac{\partial \theta}{\partial t}=\frac{1}{r}\frac{\partial}{\partial r}\left[rK(\theta)\frac{\partial \varphi}{\partial r}\right]+\frac{\partial}{\partial z}\left[K(\theta)\frac{\partial \varphi}{\partial z}\right]-\frac{\partial K(\theta)}{\partial z} \quad (1)$$

where, θ is the soil volumetric water content, cm³/cm³; r is the radial coordinate, cm; z is the vertical coordinate, cm, specifying z

downward as positive; φ is the pressure head and matric potential in saturated and unsaturated regions, cm, respectively; t is time, min; and $k(\theta)$ is the unsaturated hydraulic conductivity of the soil, cm/min.

Equation (1) involves a relationship between θ, φ, and $K(\theta)$, which is fitted in the simulation using the van Genuchten-Mualem (VG-M)[24,25] model:

$$S_e(h) = \frac{\theta - \theta_r}{\theta_s - \theta_r} = (1 + |\alpha h|^n)^{\frac{1-n}{n}} \tag{2}$$

$$K(\theta) = K_s S_e^{0.5} \left[1 - (1 - S_e^{1/m})^m\right]^2 \tag{3}$$

where, $S_e(h)$ is effective degree of saturation; θ represents the soil moisture content, cm³/cm³; θ_r is the residual soil water content, cm³/cm³; θ_s is the saturated water content, cm³/cm³; α is the reciprocal of the intake air suction, cm⁻¹; n and m are fitting parameters related to the physical characteristics of the soil (n>1, m=1–1/n); and K_s is the soil saturated hydraulic conductivity, cm/min.

2.3.2 Definite solution conditions

Considering the actual conditions of the underground porous membrane, the initial and boundary conditions for different modeling scenarios were established (Figure 3).

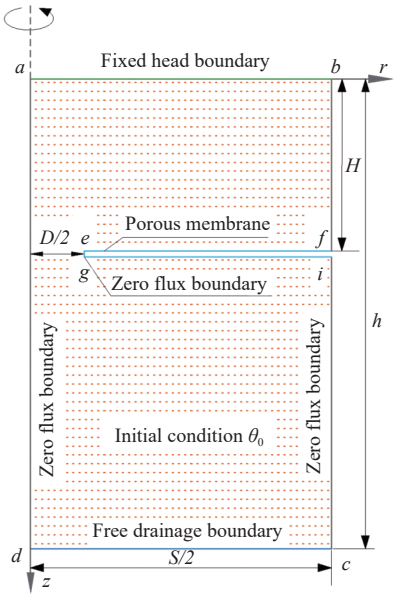

Note: ab is a constant head boundary; ad and bc are zero flux boundary; dc is free boundary; ef, gi, and eg are zero flux boundary; D/2 is half the diameter of the porous membrane; H is porous membrane burial depth; S/2 is half of the porous membrane spacing; h is the simulation depth set in this study.

Figure 3 Schematic diagram of the calculation domain for soil moisture movement in underground porous membranes

1) Initial conditions

The initial conditions for solving the basic equations of soil moisture movement can be described as follows:

$$\theta(r,z,t) = \theta_0 (0 \le r \le S/2,\ 0 \le z \le h,\ t = 0) \tag{4}$$

2) Boundary conditions

To ensure that the computational domain accurately reflected the actual conditions, the upper boundary (ab) was established as a constant head boundary in accordance with the atmospheric boundary conditions. The left and right boundaries (ad and bc) were designated as zero flux boundary conditions. The lower boundary (dc) was treated as a free boundary condition, which was aligned with the principle of free drainage. Notably, under varying field plant conditions, the spacing of porous membranes can differ significantly. The boundary settings discussed in this study primarily addressed scenarios of free infiltration with relatively large porous membrane spacing. For the lower boundary, a large enough vertical distance of 60 cm was established to ensure that the simulation results were not affected by irrigation water at the end of the simulation period. In all simulation scenarios, considering that the depth of irrigation water (ranging from 2 to 10 cm) is difficult to control and has a minimal impact on soil infiltration, the ab boundary was set as a constant head boundary for simplification in calculations when simulating the underground porous membrane.

$$\varphi_i = 2 \text{ cm} (t > 0,\ \text{ab boundary}) \tag{5}$$

Based on the aforementioned analysis, the other boundary conditions can be summarized as follows:

$$\frac{\partial \theta}{\partial z} = 0 (t > 0,\ \text{cd boundary}) \tag{6}$$

$$-K(\theta)\frac{\partial \theta}{\partial r} = 0 (t > 0,\ \text{ad, bc, ef, eg, and gi boundary}) \tag{7}$$

where, φ_i is the surface pressure head, cm.

2.3.3 Numerical solution method

The numerical solutions were obtained using the HYDRUS-2D/3D software[20,21]. The simulation area was a rectangular region with a vertical length of 60 cm and a horizontal width determined by the spacing of porous membranes. The time step was set to 0.1 minutes and the spatial step was 1 cm. Soil texture data were collected from the aeolian sandy soils in four different areas: Hulunbuir Sandy Land[26], Mu Us Sandy Land[27], Ningxia Sandy Land[28], and Gurbantunggut Desert[29]. The parameters of the Van Genuchten-Mualem model are listed in Table 3.

Table 3 The van Genuchten–Mualem model parameters of different simulated soils

Soil source	θ_r/cm³·cm⁻³	θ_s/cm³·cm⁻³	α/cm	n	K_s/cm·min⁻¹
Hulunbeier Sandy Land	0.029	0.398	0.046	1.52	0.06
Mu Us Sandy Land	0.039	0.389	0.043	2.36	0.17
Yinchuan Sandy Land	0.047	0.395	0.038	2.52	0.25
Gurbantünggüt Desert	0.046	0.366	0.037	2.90	0.31

Note: θ_r denotes soil residual water content; θ_s denotes soil saturated water content; α denotes reciprocal of intake air suction; n denotes a fitting parameter related to the physical characteristics of the soil; K_s denotes soil saturated hydraulic conductivity.

2.4 Numerical simulation scheme

Based on the actual planting conditions of the crops, the porous membrane diameter (D) was set at four values: 4, 6, 8, and 10 cm. The porous membrane spacing (S) was established at four gradients: 30, 40, 50, and 60 cm. Considering the growth requirements of crop root systems[30], plowing depth during cultivation[31], and research on the deep burial of straw for returning to the field[32], four gradients were selected for the porous membrane burial depth (H): 25, 30, 35, and 40 cm. A control group without membranes (CK) was established. In total, 272 groups of underground porous membrane infiltration simulation schemes were designed based on a multi-factor completely randomized scheme. The simulation analyzed the effects of porous membrane diameter, spacing, and burial depth on the infiltration rate and cumulative infiltration of four soil textures.

2.5 Description of estimation model for cumulative infiltration of underground porous membranes

Soil infiltration models quantitatively describe the soil infiltration process and serve as a foundation for analyzing soil

infiltration patterns. Underground porous membranes represent two-dimensional infiltration under conditions of adequate water supply, and their infiltration process can be characterized by the Kostiakov two-parameter infiltration model[33], expressed as:

$$I = Ft^{\tau} \tag{8}$$

where, I is the cumulative infiltration, L; F is the infiltration coefficient; t is the infiltration time, h; and τ is the infiltration index.

2.6 Data processing

Simulation and experimental data for various treatments, factors, and levels were compared and analyzed using Microsoft Excel 2022. Graphs were generated using Origin 2021 and Auto CAD 2020. Statistical analysis of the model errors was conducted using the root mean square error (RMSE) and Nash-Sutcliffe efficiency coefficient (NSE)[34,35]. The equations for calculating these statistical parameters are as follows:

$$\mathrm{RMSE} = \sqrt{\frac{1}{N}\sum_{i=1}^{N}(O_i - E_i)^2} \tag{9}$$

$$\mathrm{NSE} = 1 - \frac{\sum_{i=1}^{N}(O_i - E_i)^2}{\sum_{i=1}^{N}(O_i - O_m)^2} \tag{10}$$

$$R^2 = \frac{\left(N\sum_{i=1}^{N}E_iO_i - \sum_{i=1}^{N}O_i\sum_{i=1}^{N}E_i\right)^2}{\left(N\sum_{i=1}^{N}(E_i)^2 - \left(\sum_{i=1}^{N}E_i\right)^2\right)\left(N\sum_{i=1}^{N}(O_i)^2 - \left(\sum_{i=1}^{N}O_i\right)^2\right)} \tag{11}$$

where, O_i and E_i represent the measured and estimated values, respectively, O_m is the average of the measured values, and N is the total number. The closer the RMSE value is to 0 and the closer the NSE value is to 1, the smaller the deviation between the estimated and measured values and the higher the agreement between the two. R^2 is the coefficient of determination. Its value ranges from 0 to 1. The closer the R^2 value is to 1, the better the empirical model performance.

3 Results

3.1 Validation of HYDRUS-2D/3D numerical simulation

HYDRUS-2D/3D software was used to simulate schemes 1-4 (Table 2) to obtain the soil infiltration rates and cumulative infiltration of aeolian sandy soil at various time points. The simulation results were compared with the underground porous membrane test data (Table 4) to validate the reliability of the mathematical model for infiltration based on the HYDRUS-2D/3D software.

As presented in Table 4, the absolute values of the relative errors between the simulated and measured values of soil infiltration rates and cumulative infiltration at various time intervals ranged from 0.52% to 8.50%, with an average of 4.51%. The RMSE for the infiltration rate was 0.151 L/h, and the NSE was 0.994. The RMSE for cumulative infiltration was 0.019 L, with a Nash-Sutcliffe efficiency coefficient of 0.991. These results indicate that the mathematical model developed in this study is accurate and that the use of HYDRUS-2D/3D software to simulate the infiltration process of underground porous membranes is reliable.

Table 4 Comparison of simulated and measured values of soil infiltration rate and cumulative infiltration at different infiltration times

Scheme number	Time/h	Soil infiltration rate			Cumulative infiltration		
		Measured value/ L·h^{-1}	Simulated value/ L·h^{-1}	Relative error/%	Measured value/ L·h^{-1}	Simulated value/ L·h^{-1}	Relative error/%
1	0.05	58.24	59.00	–1.30	11.94	11.59	3.04
	0.12	42.62	40.34	5.66	20.24	19.59	3.32
	0.25	9.64	9.06	6.38	23.81	23.22	2.53
	0.35	7.56	8.26	–8.50	25.70	25.18	2.08
2	0.05	164.80	163.95	0.52	11.94	11.59	3.04
	0.12	131.49	111.99	3.77	20.24	19.59	3.32
	0.25	116.21	13.32	6.48	23.81	23.22	2.53
	0.40	47.78	13.13	4.00	25.70	25.18	2.08
3	0.05	110.34	104.70	5.38	7.90	7.43	6.33
	0.12	61.41	81.19	5.89	12.48	12.05	3.53
	0.25	15.28	16.13	5.29	14.57	14.25	2.27
	0.40	14.93	16.01	6.77	15.30	15.03	1.80
4	0.05	244.23	236.05	3.47	16.87	16.70	1.02
	0.12	168.49	161.44	4.37	28.75	28.14	2.16
	0.25	30.21	28.33	6.64	38.33	37.86	1.25
	0.40	25.87	25.03	3.33	39.20	38.70	1.30

3.2 Impact of various influencing factors on infiltration rate

3.2.1 Influence of porous membrane diameter on infiltration rate

A single-factor analysis of the porous membrane diameter was conducted under various combinations of the soil-saturated hydraulic conductivity, porous membrane burial depth, and spacing. Figure 4 illustrates the variation in soil infiltration rates for the four types of aeolian sandy soils with different porous membrane diameters.

As shown in Figure 4, the initial soil infiltration rates across all treatments were relatively high. However, over time, these infiltration rates decreased sharply before gradually stabilizing and ultimately reaching a steady infiltration rate. By the end of the infiltration period, the minimum decrease in the infiltration rate under the different porous membrane diameters was 2.86 times lower than that of the CK treatment. This reduction is likely attributable to the obstructive effect of underground porous membranes, which impede water infiltration. The saturated hydraulic conductivity of the soil significantly influences the soil infiltration rate. When the porous membrane diameter, burial depth, and spacing were held constant, the soil infiltration rate increased with an increase in saturated hydraulic conductivity. For instance, at D=4 cm, H=30 cm, and S=40 cm, the infiltration rates at the end of irrigation for K_s values of 0.17, 0.25, and 0.31 cm/min were 3.28, 5.09, and 6.58 times greater, respectively, than those for K_s= 0.06 cm/min. The analysis attributes this phenomenon to the relationship between saturated hydraulic conductivity and soil permeability; specifically, a higher saturated hydraulic conductivity leads to increased soil permeability and, consequently, a faster water infiltration rate. Further analysis revealed that the diameter of the porous membrane also significantly affected the soil infiltration rate. When the saturated hydraulic conductivity, burial depth, and spacing were held constant, the soil infiltration rate increased with an increase in the diameter of the porous membrane. For instance, when K_s=0.06 cm/min, H=30 cm, and S=40 cm, the infiltration rates at the end of irrigation for membrane diameters of D=4, 6, and 8 cm decreased by 163.2%, 70.5%, and 54.4%, respectively, compared with the infiltration rate for D=10 cm. This can be attributed to the

fact that the pores in the underground membrane act as infiltration interfaces for moisture. As the diameter of the porous membrane increased, the number of channels available for moisture to enter the soil also increased, resulting in a higher soil infiltration rate.

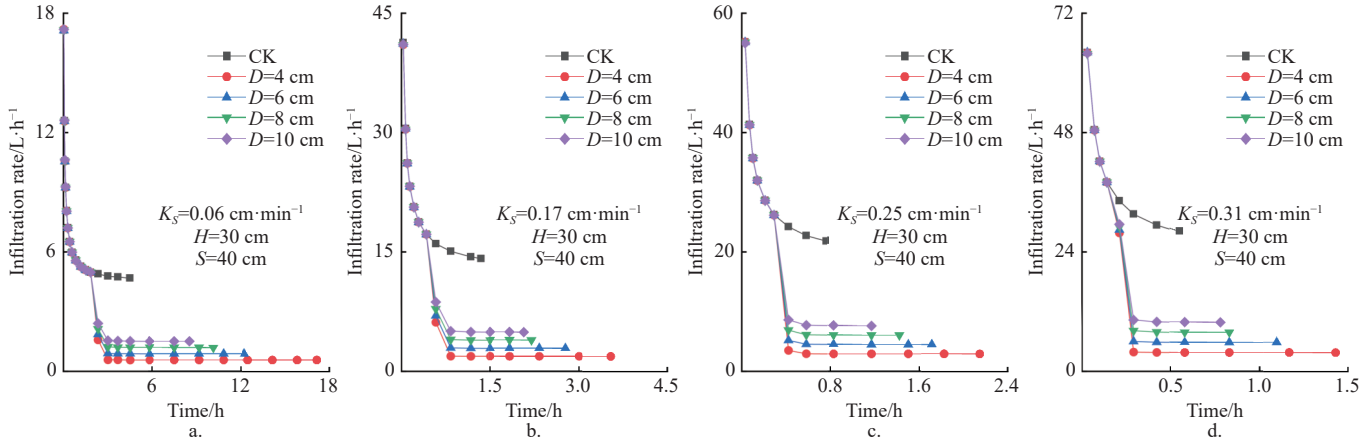

Note: CK is control treatment; K_s is soil saturated hydraulic conductivity; D is porous membrane diameter; H is porous membrane burial depth; S is porous membrane spacing. Same as below.

Figure 4 Relationship between soil infiltration rate and time for four types of aeolian sandy soils under different porous membrane diameters

3.2.2 Influence of porous membrane burial depth on soil infiltration rate

A single-factor analysis of the burial depth of the porous membrane was conducted under various combinations of the soil-saturated hydraulic conductivity, porous membrane diameter, and spacing. Figure 5 illustrates the variation in soil infiltration rates at different burial depths of the porous membrane for the four aeolian sandy soil types.

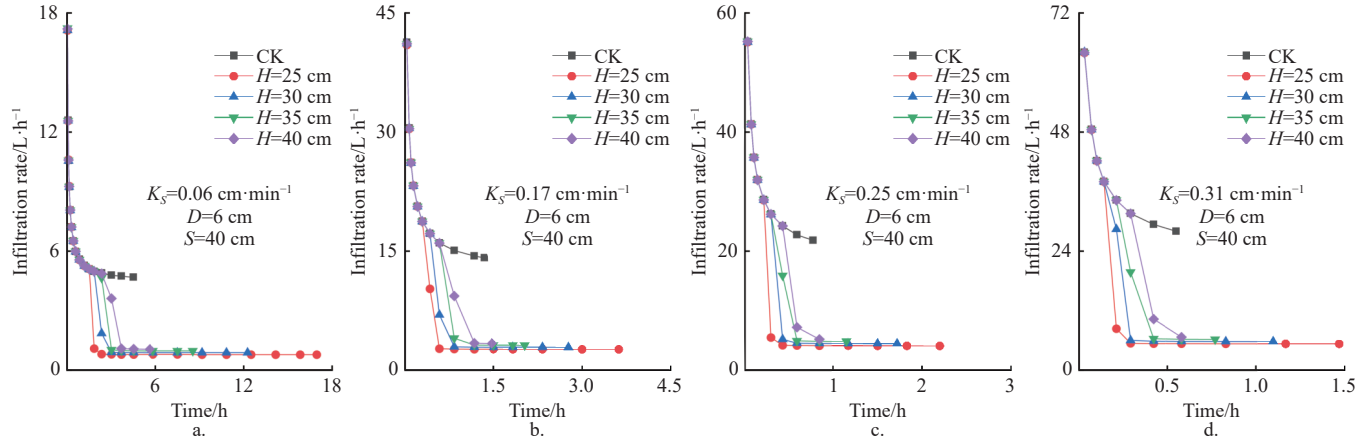

Figure 5 Relationship between soil infiltration rate and time for four types of aeolian sandy soils under different porous membrane burial depths

As illustrated in Figure 5, during the initial stage of infiltration, the soil water potential gradient was relatively steep, resulting in higher infiltration rates across all treatments, with nearly overlapping infiltration curves. As the infiltration time progressed, the change curve of the buried depth of the different porous membranes began to diverge from that of the CK treatment, with the change range varying between 4.20 and 6.00 times by the end of the infiltration period. This divergence is attributed to the influence of the porous membrane on the water infiltration at this stage. The burial depth of porous membranes significantly affected the soil infiltration rates. When the saturated hydraulic conductivity, porous membrane diameter, and spacing were held constant, the soil infiltration rate increased with increasing burial depth of porous membranes. For instance, when K_s=0.25 cm/min, D=4 cm, and S=40 cm, the infiltration rates at the end of irrigation for H=25, 30, and 35 cm were reduced by 27.5%, 16.6%, and 7.5%, respectively, compared with the infiltration rate at H=40 cm. This reduction occurred because, as the burial depth of porous membrane increased, the soil water potential gradient in the soil layer above the membrane also increased, thereby enhancing the soil infiltration rate.

3.2.3 Influence of porous membrane spacing on soil infiltration rate

Single-factor analysis of S was conducted under various combinations of K_s, D, and H. Figure 6 illustrates the variation in soil infiltration rates at different S values for the four types of aeolian sandy soils.

As illustrated in Figure 6, under the four types of aeolian sandy soil conditions, when moisture had not yet reached the porous membrane, the variation in the infiltration rate over time for different porous membrane spacings was consistent with that of the CK treatment. However, once moisture migrated through the porous membrane, the infiltration rate fluctuated significantly across different porous membrane spacings compared with the CK treatment. The decrease was substantial, with a change range varying between 2.98 and 11.49 times the original values. This

phenomenon is likely due to the porous membrane disrupting the continuity of the capillary pores in the soil, thereby reducing the soil moisture infiltration rate. Furthermore, when the saturated hydraulic conductivity, porous membrane diameter, and burial depth were kept constant, the soil infiltration rate slightly increased as the spacing of porous membranes increased. For instance, when K_s=0.17 cm/min, D=6 cm, and H=30 cm, the infiltration rates at the end of irrigation for spacings of S=30, 40, and 50 cm were reduced by 14.4%, 4.9%, and 1.3%, respectively, compared with the infiltration rate at S=60 cm. This phenomenon may be attributed to the fact that a smaller porous membrane spacing leads to an earlier convergence of the wetting fronts, resulting in a rapid increase in the local moisture content of the soil at the upper interface of the porous membrane, which in turn reduces the soil infiltration rate.

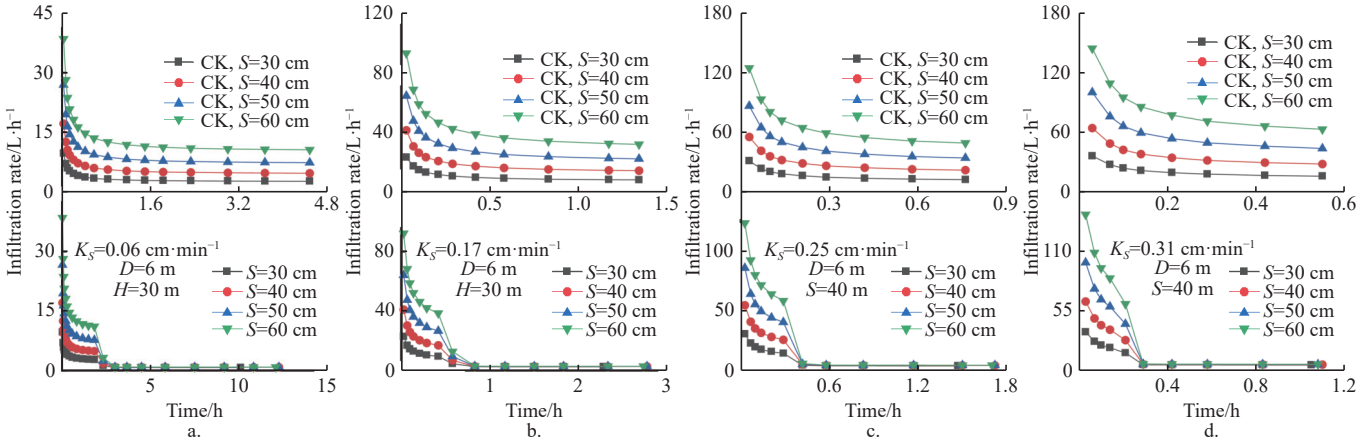

Figure 6 Relationship between soil infiltration rate and time for four types of aeolian sandy soils under different porous membrane spacings

3.3 Establishment and evaluation of steady infiltration rate model

From 256 sets of simulations involving underground porous membrane infiltration, soil steady infiltration rates were obtained under various combinations of influencing factors. The relationship curves between the soil steady infiltration rates and factors, such as saturated hydraulic conductivity, porous membrane spacing, diameter, and burial depth are illustrated in Figure 7.

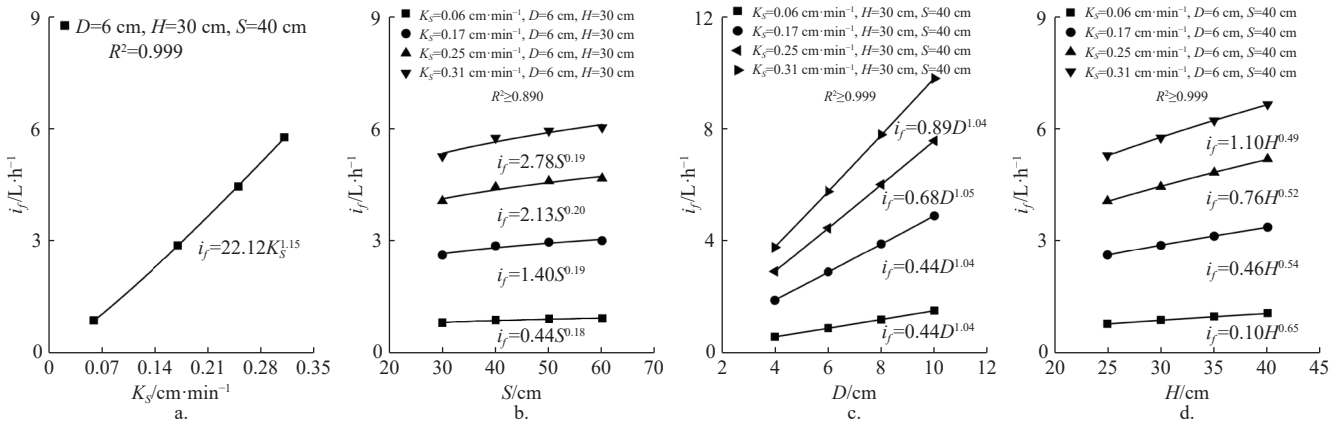

Note: R^2 is the coefficient of determination; i_f is the steady infiltration rate; K_s is soil saturated hydraulic conductivity; D is porous membrane diameter; H is porous membrane burial depth; S is porous membrane spacing.

Figure 7 The functional relationship between steady infiltration rate and saturated hydraulic conductivity, porous membrane diameter, porous membrane burial depth, and porous membrane spacing

As illustrated in Figure 7, the soil steady infiltration rate exhibited a strong power function relationship with the saturated hydraulic conductivity, porous membrane spacing, diameter, and burial depth (R^2≥0.890). Consequently, this study proposed an estimation model for the steady infiltration rate based on the saturated hydraulic conductivity, porous membrane spacing, diameter, and burial depth.

$$i_f = aK_s^b D^c H^d S^e \tag{12}$$

where, i_f represents the steady infiltration rate, L/h; a is the infiltration coefficient; and b, c, d, and e are the fitting indices.

Using Equation (12), based on the infiltration simulation results, the infiltration coefficient and infiltration index values were fitted to determine the expression for the soil steady infiltration rate, as follows:

$$i_f = 0.209K_s^{1.14} D^{1.04} H^{0.48} S^{0.30},\ R^2 = 0.997 \tag{13}$$

To evaluate the applicability and reliability of the steady infiltration rate model developed in this study, this study utilized the measured values from the underground porous membrane infiltration tests (Schemes 5-8) to assess the accuracy of Equation (13). The relevant statistical error indicators are listed in Table 5.

As presented in Table 5, the relative error between the calculated and measured values is relatively small, ranging from –5.53 to 0.68. The RMSE was 0.143 L/h, which was close to 0, and the NSE was 0.995, which approached 1. This indicates strong consistency between the calculated and measured values when using Equation (13) to estimate the soil steady infiltration rate under

various combinations of saturated hydraulic conductivity, porous membrane diameter, spacing, and burial depth.

Table 5 Validation of the empirical model for steady infiltration rate of underground porous membrane

Scheme	Measured value	Calculated value	Relative error/%	RMSE/ L·h^{-1}	NSE
5	4.90	5.18	–5.53	0.143	0.995
6	8.28	8.64	–4.17		
7	9.93	10.12	–1.83		
8	11.77	11.69	0.68		

Note: Scheme 5 to 8 was tested according to the indoor test scheme (Table 2), and the estimation model of the soil steady infiltration rate of underground porous membrane was verified; RMSE denotes the root mean square error; NSE denotes the Nash-Sutcliffe efficiency coefficients.

3.4 Influence of different factors on cumulative infiltration

3.4.1 Effect of porous membrane diameter on cumulative infiltration

The effect of the porous membrane diameter on cumulative infiltration was examined under consistent conditions of soil-saturated hydraulic conductivity, porous membrane spacing, and burial depth. Figure 8 illustrates the variation in cumulative infiltration over time for the four different diameters of porous membranes.

As illustrated in Figure 8, the soil cumulative infiltration gradually increased over time, demonstrating a strong power–function relationship. During the initial stage of infiltration, there was minimal difference in cumulative infiltration between the various porous membrane diameter treatments and the CK treatment. However, as water passed through the porous membrane, the cumulative infiltration under the different porous membrane diameter treatments was lower than that of the CK treatment. Soil-saturated hydraulic conductivity significantly influenced the cumulative infiltration. Under consistent conditions of porous membrane diameter, burial depth, and spacing, the cumulative infiltration increased with higher saturated hydraulic conductivity at the same infiltration moment. For instance, when D=6 cm, H=30 cm, and S=40 cm, using K_s=0.06 cm/min as the basis, as K_s increased to 0.17, 0.25, and 0.31 cm/min, the cumulative infiltration reductions of 17.40%, 20.25%, and 33.16%, respectively, were observed at the end of the infiltration. This phenomenon occurs because the permeability of the soil is enhanced, leading to accelerated water movement and a greater volume of water infiltrating the soil layer per unit of time. Furthermore, when the saturated hydraulic conductivity, burial depth of the porous membrane, and spacing between membranes were held constant, cumulative infiltration increased with an increase in the diameter of the porous membrane. For instance, with a saturated hydraulic conductivity of K_s=0.17 cm/min, at the end of irrigation, the cumulative infiltration for a diameter of D=4 cm was reduced by 3.61%, 6.55%, and 9.75% compared with diameters of D=6, 8, and 10 cm, respectively. This reduction may be attributed to the fact that increasing the pore diameter of the membrane expanded the infiltration interface area and increased the water infiltration pathways, resulting in a greater volume of water passing through the membrane pores within the same time.

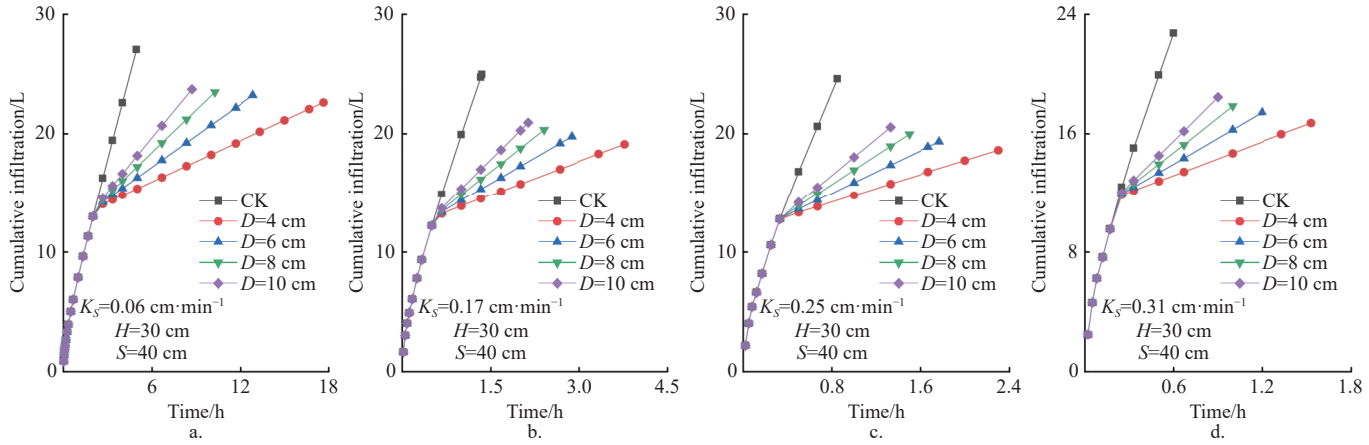

Figure 8 Relationship between cumulative infiltration and time under different porous membrane diameters

3.4.2 Effect of porous membrane burial depth on cumulative infiltration

The impact of the porous membrane burial depth on the cumulative infiltration was analyzed under identical conditions of soil-saturated hydraulic conductivity, porous membrane diameter, and spacing. Figure 9 illustrates the variation curves of the cumulative infiltration over time for four different porous membrane burial depths.

As illustrated in Figure 9, the relationship between the saturated hydraulic conductivity and cumulative infiltration for the four types of aeolian sandy soils closely resembled that depicted in Figure 8. The burial depth of the porous membrane significantly influenced the cumulative infiltration. Under conditions of constant saturated hydraulic conductivity, porous membrane diameter, and spacing, cumulative infiltration increased with the burial depth of the porous membrane at the same infiltration time. For instance, when K_s= 0.25 cm/min, D=6 cm, and S=40 cm, using H=25 cm as a basis, as H increased to 30, 35, and 40 cm at t=1 h (by which time the wetting front of each treatment has passed through the pore membrane), cumulative infiltration increased by 15.07%, 29.40%, and 42.90%, respectively. This increase may be attributed to the elevated upper water pressure in the soil layer above the porous membrane, which enhances the soil pressure potential.

3.4.3 Effect of porous membrane spacing on cumulative infiltration

The influence of porous membrane spacing on cumulative infiltration was analyzed under identical conditions of soil-saturated hydraulic conductivities, porous membrane diameters, and burial depths. Figure 10 illustrates the variation curves of the cumulative infiltration over time for the four different porous-membrane spacing conditions.

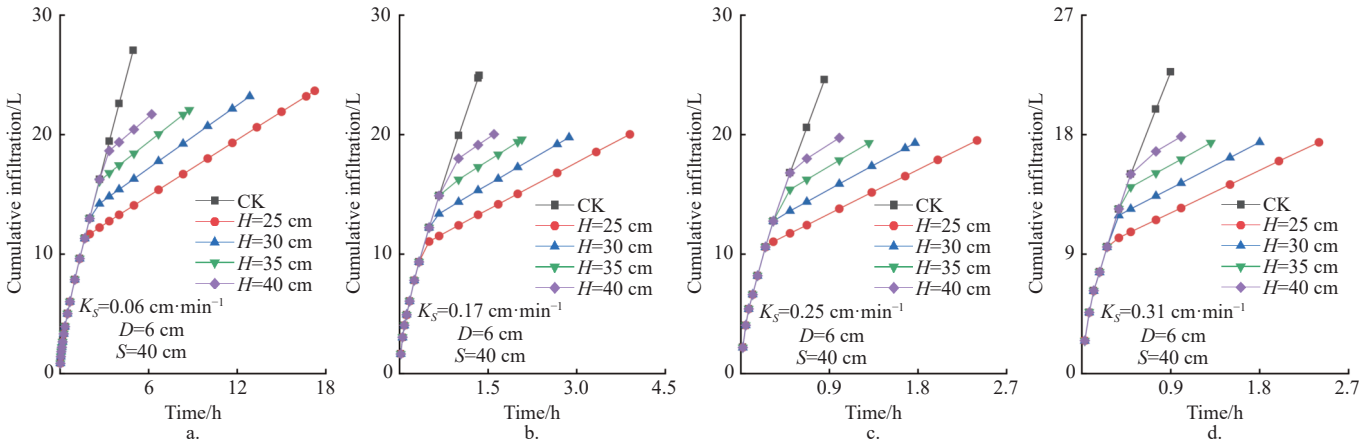

Figure 9 Relationship between cumulative infiltration and time under different porous membrane burial depths

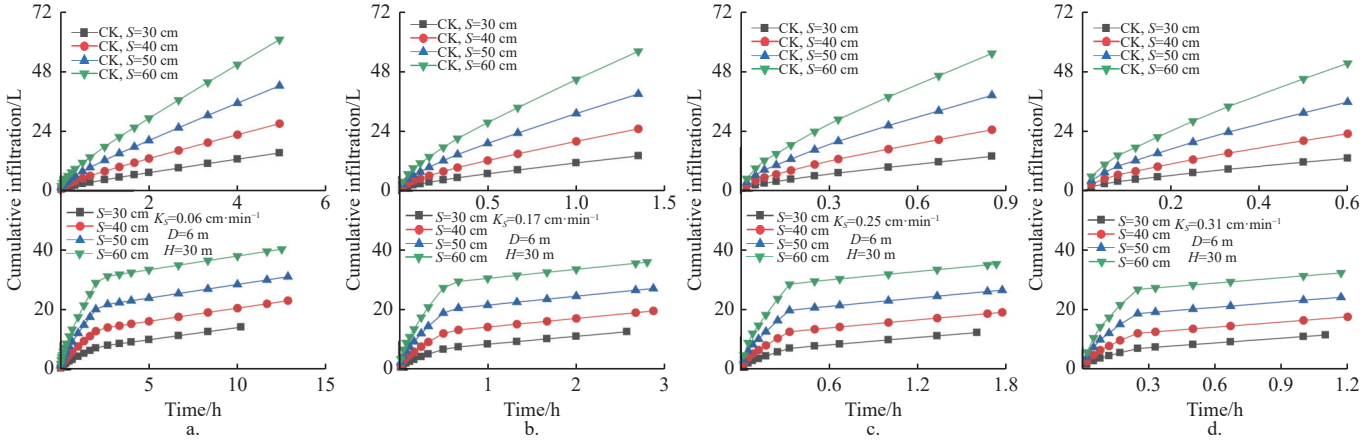

Figure 10 Relationship between cumulative infiltration and time under different porous membrane spacings

As illustrated in Figure 10, under the conditions of the four types of aeolian sandy soils, the cumulative infiltration during the initial stage of infiltration for the various porous membrane spacing treatments exhibited a trend similar to that of the CK treatment. Once water passed through the membrane pores, the cumulative infiltration variation pattern was as follows: CK>60 cm>50 cm>40 cm>30 cm. This phenomenon can be attributed to the water-retaining effect of the porous membrane, which enhanced the water-holding capacity of the upper soil layer and significantly reduced the volume of water infiltrated through the porous membrane. When the saturated hydraulic conductivity, porous membrane diameter, and burial depth were kept constant, cumulative infiltration increased as the spacing between the porous membranes increased. For instance, with K_s=0.17 cm/min, D=6 cm, and H=30 cm, using S of 30 cm as a basis, increasing the spacing to 40, 50, and 60 cm resulted in cumulative infiltration increases of 1.67, 2.53, and 3.57 times, respectively, at t=1.0 h. This phenomenon may be attributed to the convergence of wetting fronts during infiltration. As the spacing increased, convergence occurred later, allowing the soil surrounding the membrane pores to maintain a higher hydraulic gradient for an extended period. This in turn promoted sustained water infiltration and enhanced cumulative infiltration. Conversely, this effect diminishes with reduced spacing.

3.5 Establishment and evaluation of cumulative infiltration model

Through a numerical analysis of the factors influencing the cumulative infiltration of underground porous membranes, it can be concluded that the porous membrane diameter, burial depth, spacing, and infiltration time significantly affect the cumulative infiltration. These factors are critical and must be considered when establishing a model. Based on 256 sets of simulation results, aeolian sandy soils with four different textures were fitted using Equation 8. The fitting results for the F and τ values are presented in Tables 6-9.

By analyzing Tables 6, 7, 8, and 9, it can be concluded that in various simulation scenarios involving different combinations of influencing factors, R^2≥0.836. This indicates that the Kostiakov infiltration model effectively describes the evolution of cumulative infiltration of the underground porous membrane over time. The impact of different factors on the infiltration index (τ) was minimal, with τ values fluctuating between 0.38 and 0.62, demonstrating only slight variation. Considering the model simplification, τ was calculated to be 0.51 using the averaging method. Substituting τ=0.51 into Equation (8), it can be further expressed using Equation (8) as follows:

$$I = Ft^{0.51} \tag{14}$$

where, F is the infiltration coefficient.

Furthermore, the porous membrane diameter, burial depth, and spacing influence the infiltration coefficient (F). The variation trend shows that F increases with the increase in the diameter, burial depth, and spacing of the porous membrane (Figure 11).

As illustrated in Figure 11, a strong power function relationship existed between the infiltration coefficient (F) and porous membrane diameter, burial depth, and spacing (R^2≥0.974). The specific expression is as follows:

Table 6 Fitting values of infiltration parameters for four types of aeolian sandy soils under the condition of different porous membrane burial depth, porous membrane spacing, and porous membrane diameter of 4 cm

D/cm	*H*/cm	*S*/cm	Aeolian sandy soil (γ=0.06 g·cm^{-1})			Aeolian sandy soil (γ=0.17 g·cm^{-1})			Aeolian sandy soil (γ=0.25 g·cm^{-1})			Aeolian sandy soil (γ=0.31 g·cm^{-1})		
			F	τ	R^2	*F*	τ	R^2	*F*	τ	R^2	*F*	τ	R^2
4	25	30	3.80	0.48	0.981	6.97	0.44	0.976	8.48	0.42	0.974	8.90	0.40	0.978
		40	6.29	0.43	0.964	11.03	0.39	0.956	13.19	0.36	0.945	13.59	0.34	0.951
		50	9.39	0.40	0.939	16.12	0.36	0.951	19.09	0.33	0.898	19.39	0.31	0.903
		60	13.16	0.38	0.901	22.32	0.34	0.874	26.28	0.31	0.851	26.44	0.28	0.853
	30	30	4.06	0.52	0.975	7.81	0.48	0.968	9.63	0.46	0.965	10.25	0.44	0.967
		40	6.80	0.48	0.947	12.62	0.44	0.934	15.25	0.41	0.928	16.29	0.40	0.920
		50	10.30	0.46	0.900	18.83	0.42	0.895	22.52	0.39	0.855	23.91	0.38	0.873
		60	14.56	0.45	0.877	26.39	0.41	0.866	31.34	0.38	0.851	33.17	0.36	0.836
	35	30	4.31	0.55	0.971	8.62	0.52	0.966	10.83	0.51	0.964	11.78	0.49	0.958
		40	7.42	0.53	0.938	14.57	0.50	0.936	18.08	0.48	0.930	19.45	0.46	0.919
		50	11.38	0.52	0.912	22.17	0.49	0.914	27.33	0.47	0.904	29.17	0.45	0.889
		60	16.21	0.52	0.895	31.41	0.48	0.899	38.55	0.46	0.887	40.99	0.44	0.868
	40	30	4.54	0.54	0.979	9.41	0.56	0.980	12.21	0.55	0.970	13.57	0.54	0.969
		40	7.94	0.57	0.965	16.27	0.55	0.967	21.02	0.54	0.951	23.24	0.53	0.951
		50	12.31	0.57	0.955	25.02	0.54	0.957	32.34	0.53	0.940	35.72	0.52	0.942
		60	17.63	0.57	0.948	35.73	0.54	0.953	46.07	0.53	0.932	50.80	0.52	0.934

Note: *D* denotes porous membrane diameter; *H* denotes porous membrane burial depth; *S* denotes porous membrane spacing; *F* denotes the infiltration coefficient; τ denotes the infiltration index; R^2 denotes the coefficient of determination. Same as below.

Table 7 Fitting values of infiltration parameters for four types of aeolian sandy soils under the condition of different porous membrane burial depth, porous membrane spacing, and porous membrane diameter of 6 cm

D/cm	*H*/cm	*S*/cm	Aeolian sandy soil (γ=0.06 g·cm^{-1})			Aeolian sandy soil (γ=0.17 g·cm^{-1})			Aeolian sandy soil (γ=0.25 g·cm^{-1})			Aeolian sandy soil (γ=0.31 g·cm^{-1})		
			F	τ	R^2	*F*	τ	R^2	*F*	τ	R^2	*F*	τ	R^2
6	25	30	4.05	0.52	0.990	7.72	0.48	0.989	9.56	0.46	0.987	10.32	0.45	0.985
		40	6.67	0.48	0.976	12.15	0.42	0.970	14.66	0.41	0.966	15.52	0.39	0.964
		50	9.92	0.44	0.951	17.63	0.40	0.937	20.92	0.37	0.929	21.91	0.35	0.923
		60	13.85	0.42	0.917	24.24	0.38	0.901	28.47	0.35	0.888	29.60	0.33	0.879
	30	30	4.29	0.55	0.989	8.51	0.52	0.984	10.72	0.50	0.982	11.62	0.49	0.982
		40	7.19	0.52	0.966	13.68	0.48	0.960	16.82	0.45	0.955	18.32	0.45	0.948
		50	10.86	0.50	0.934	20.24	0.46	0.928	24.58	0.43	0.918	26.65	0.42	0.908
		60	15.35	0.49	0.906	28.21	0.44	0.901	33.97	0.41	0.887	36.74	0.40	0.875
	35	30	4.47	0.57	0.988	9.12	0.55	0.986	11.86	0.54	0.982	13.16	0.53	0.978
		40	7.68	0.56	0.961	15.27	0.52	0.963	19.80	0.52	0.957	21.75	0.51	0.950
		50	11.78	0.54	0.945	23.03	0.51	0.944	29.85	0.50	0.935	32.54	0.49	0.926
		60	16.74	0.54	0.929	32.46	0.50	0.928	42.05	0.50	0.919	45.65	0.48	0.907
	40	30	4.64	0.59	0.992	9.88	0.58	0.992	12.78	0.57	0.987	14.35	0.56	0.987
		40	8.12	0.59	0.984	17.11	0.57	0.982	22.55	0.57	0.972	25.25	0.56	0.973
		50	12.59	0.59	0.979	26.34	0.57	0.976	34.80	0.56	0.964	38.65	0.55	0.962
		60	18.07	0.58	0.974	37.56	0.56	0.971	49.61	0.56	0.957	54.95	0.55	0.955

$$F = p_1 K_s^{q^1} D^{q^2} H^{q^3} S^{q^4} \tag{15}$$

where, p_1, q^1, q^2, q^3, and q^4 are parameters to be determined.

Using multivariate nonlinear regression, 256 sets of underground porous membrane simulation data were fitted to obtain the values of q^1, q^2, q^3, and q^4, thereby deriving a calculation formula for *F*.

$$F = 0.0012 K_s^{0.59} D^{0.18} H^{0.99} S^{1.81} \tag{16}$$

Based on this, by substituting Equation (16) into Equation (14), a simplified model for cumulative infiltration was ultimately developed based on the Kostiakov infiltration model:

$$\begin{aligned} I &= 0.0012 K_s^{0.59} D^{0.18} H^{0.99} S^{1.81} t^{0.51} \\ R^2 &= 0.990 \end{aligned} \tag{17}$$

Experimental data from schemes 5 to 8 of the underground porous membrane testing were used to evaluate the reliability of the cumulative infiltration estimation model for underground porous membranes. The calculated values of cumulative infiltration at different times were compared with the measured values, as shown in Figure 12.

As illustrated in Figure 12, the trend of the calculated values from the underground porous membrane cumulative infiltration estimation model closely aligns with the experimentally measured values. Statistical analysis of the model errors using the RMSE and NSE indicators revealed that the RMSE was approximately 0 (RMSE=0.028 L) and the NSE was nearly 1 (NSE=0.999). The calculated values derived from the established model exhibited only a minor discrepancy when compared with the experimental values, indicating that the developed estimation model can accurately represent the cumulative infiltration of underground porous membrane irrigation.

Table 8 Fitting values of infiltration parameters for four types of aeolian sandy soils under the condition of different porous membrane burial depth, porous membrane spacing, and porous membrane diameter of 8 cm

D/cm	*H*/cm	*S*/cm	Aeolian sandy soil (γ=0.06 g·cm^{-1})			Aeolian sandy soil (γ=0.17 g·cm^{-1})			Aeolian sandy soil (γ=0.25 g·cm^{-1})			Aeolian sandy soil (γ=0.31 g·cm^{-1})		
			F	τ	R^2	*F*	τ	R^2	*F*	τ	R^2	*F*	τ	R^2
8	25	30	4.23	0.55	0.995	8.34	0.52	0.994	10.50	0.50	0.993	11.40	0.49	0.993
		40	7.00	0.51	0.985	13.09	0.46	0.981	16.05	0.44	0.978	17.22	0.43	0.975
		50	10.39	0.48	0.960	18.85	0.43	0.954	22.68	0.40	0.947	24.10	0.39	0.941
		60	14.47	0.46	0.929	25.76	0.41	0.922	30.60	0.38	0.910	32.34	0.37	0.900
	30	30	4.42	0.57	0.996	9.00	0.55	0.993	11.47	0.53	0.992	12.79	0.53	0.990
		40	7.45	0.54	0.980	14.62	0.51	0.974	18.27	0.49	0.969	20.23	0.48	0.963
		50	11.24	0.52	0.955	21.58	0.48	0.948	26.63	0.46	0.938	29.40	0.46	0.929
		60	16.01	0.52	0.929	29.97	0.47	0.924	36.65	0.44	0.909	40.52	0.44	0.900
	35	30	4.57	0.59	0.995	9.62	0.57	0.993	12.44	0.56	0.992	14.90	0.55	0.990
		40	7.89	0.57	0.982	16.13	0.55	0.977	20.65	0.54	0.974	22.84	0.53	0.969
		50	12.08	0.56	0.966	24.33	0.53	0.961	30.98	0.52	0.956	33.94	0.51	0.948
		60	17.23	0.56	0.954	34.29	0.52	0.948	43.43	0.51	0.941	47.38	0.50	0.931
	40	30	4.68	0.60	0.996	10.12	0.59	0.997	13.37	0.59	0.994	15.12	0.58	0.993
		40	8.20	0.59	0.992	17.47	0.58	0.991	23.14	0.58	0.986	25.92	0.57	0.983
		50	12.50	0.58	0.991	26.83	0.57	0.985	35.51	0.57	0.977	39.53	0.56	0.974
		60	18.20	0.59	0.984	38.26	0.57	0.981	50.83	0.57	0.974	56.59	0.56	0.971

Table 9 Fitting values of infiltration parameters for four types of aeolian sandy soils under the condition of different porous membrane burial depth, porous membrane spacing, and porous membrane diameter of 10 cm

D/cm	*H*/cm	*S*/cm	Aeolian sandy soil (γ=0.06 g·cm^{-1})			Aeolian sandy soil (γ=0.17 g·cm^{-1})			Aeolian sandy soil (γ=0.25 g·cm^{-1})			Aeolian sandy soil (γ=0.31 g·cm^{-1})		
			F	τ	R^2	*F*	τ	R^2	*F*	τ	R^2	*F*	τ	R^2
10	25	30	4.37	0.57	0.998	8.86	0.54	0.998	11.34	0.53	0.996	12.43	0.52	0.995
		40	7.24	0.53	0.989	13.83	0.49	0.989	17.33	0.47	0.984	18.54	0.46	0.985
		50	10.73	0.50	0.972	19.73	0.45	0.969	24.00	0.43	0.965	25.62	0.41	0.960
		60	14.93	0.48	0.946	26.76	0.43	0.943	32.07	0.40	0.934	34.06	0.38	0.925
	30	30	4.53	0.59	0.998	9.47	0.57	0.997	12.23	0.56	0.996	13.59	0.55	0.995
		40	7.66	0.56	0.989	15.25	0.53	0.985	19.63	0.52	0.978	21.38	0.50	0.977
		50	11.56	0.54	0.969	22.33	0.50	0.964	28.63	0.49	0.951	30.78	0.47	0.950
		60	16.28	0.52	0.949	30.87	0.48	0.943	39.53	0.48	0.925	42.19	0.46	0.923
	35	30	4.64	0.60	0.998	9.92	0.58	0.997	12.92	0.58	0.997	14.55	0.57	0.996
		40	8.03	0.58	0.990	16.85	0.57	0.985	21.38	0.55	0.985	23.74	0.54	0.981
		50	12.37	0.57	0.979	25.49	0.55	0.971	33.02	0.54	0.969	35.17	0.52	0.963
		60	17.61	0.57	0.970	35.97	0.55	0.960	46.44	0.54	0.956	48.87	0.51	0.947
	40	30	4.72	0.61	0.997	10.31	0.60	0.999	13.64	0.60	0.998	15.50	0.59	0.997
		40	8.26	0.60	0.995	17.78	0.59	0.995	23.53	0.58	0.991	26.52	0.58	0.990
		50	12.83	0.59	0.992	27.65	0.59	0.991	35.90	0.58	0.982	40.37	0.57	0.982
		60	18.39	0.59	0.990	39.44	0.58	0.987	51.22	0.57	0.978	57.66	0.57	0.979

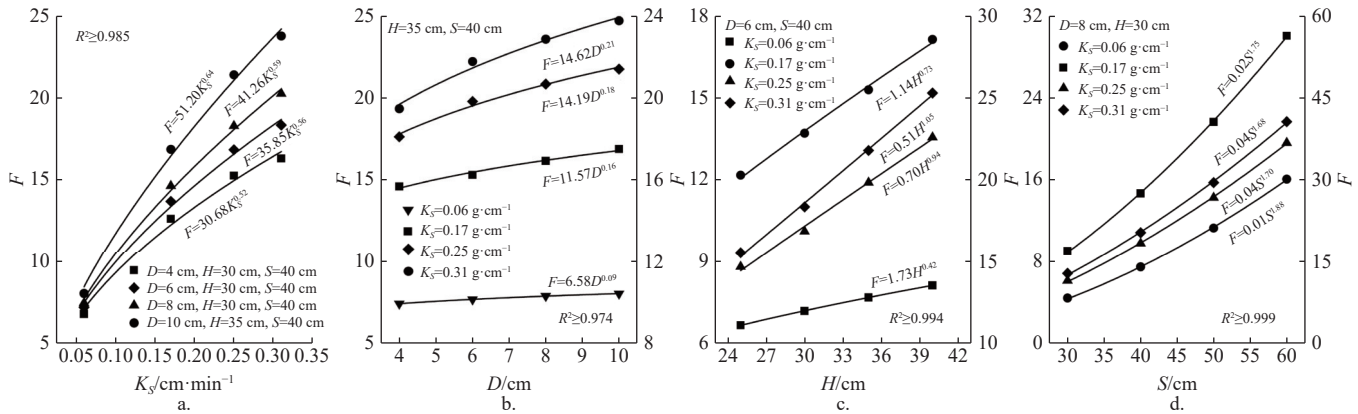

Note: R^2 is the coefficient of determination; *F* is the infiltration coefficient; K_s is soil saturated hydraulic conductivity; *D* is porous membrane diameter; *H* is porous membrane burial depth; *S* is porous membrane spacing.

Figure 11 Relationship curves of *F* with *D*, *H*, and *S* for four types of aeolian sandy soils

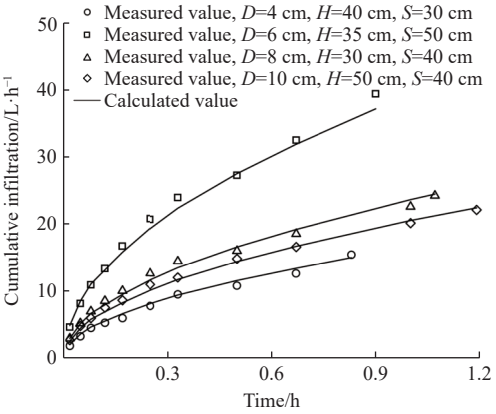

Figure 12 Comparison of measured and calculated cumulative infiltration

4 Discussion

4.1 Influence of underground porous membranes on infiltration rate and cumulative infiltration

Soil infiltration characteristics are a crucial manifestation of soil hydraulic conductivity, with infiltration rate and cumulative infiltration serving as key parameters that effectively reflect the dynamic process of soil moisture movement[36]. Previous studies have demonstrated that the presence of underground barriers significantly affects water infiltration[37-39]. In recent years, underground porous membrane technology has been increasingly applied to agricultural production engineering. This technology is low-cost, recyclable, easily integrated with other water-saving technologies, and offers significant benefits. In this study, it can be observed that, under four different aeolian sandy soil conditions, the soil water potential gradient was relatively large during the initial infiltration stage, resulting in a high initial infiltration rate. However, as the infiltration process progressed, the soil infiltration rate sharply decreased and gradually stabilized, ultimately reaching a steady infiltration rate. This observation aligns with the findings of Cheng et al.[40] regarding the characteristics of water infiltration in fractured soils subjected to drying-wetting cycles. When the moisture had not yet reached the position of the porous membrane, the infiltration rate and cumulative infiltration curves for all the treated soils were relatively steep and nearly overlapped. As the infiltration time progressed, following the movement of water through the porous membrane, the variation curves of the soil infiltration rate and cumulative infiltration under the porous membrane treatment increasingly diverged from those under the CK treatment, and the minimum decrease in soil infiltration rate of the porous membrane treatment was 2.86 times that of the CK treatment. This discrepancy may be attributed to the porous membrane disrupting the continuity of the soil capillary pores, which began to impede moisture infiltration, thereby slowing the water infiltration rate and leading to a permeability-blocking effect. This observation was consistent with the findings of Zhao et al.[41] on the patterns of water infiltration under deep straw burial methods and aligns with the results of Yao et al.[42] and Cao et al.[43]

4.2 Influence of different factors on infiltration rate and cumulative infiltration

Soil texture, porous membrane diameter, spacing of porous membranes, and porous membrane burial depth significantly affected the soil infiltration rate and cumulative infiltration. The analysis indicated that both the soil infiltration rate and cumulative infiltration increased as soil-saturated hydraulic conductivity increased. This phenomenon can be attributed to the fact that a higher saturated hydraulic conductivity signifies enhanced soil permeability, resulting in a faster rate of water infiltration and greater volume of water entering the soil over a given time[11]. In addition, porous membrane diameter significantly affected the soil infiltration rate. After the water passed through the membrane, both the soil infiltration rate and cumulative infiltration increased with larger porous membrane diameters. This is because the membrane pores act as infiltration interfaces for water. A larger pore area provides more pathways for water to enter the soil, leading to a greater volume of water infiltrating the soil within the same time, thereby resulting in a higher soil infiltration rate. This aligns with the findings of Fan et al.[44], who investigated the effect of the membrane pore diameter on soil infiltration rates under membrane pore irrigation conditions. The soil infiltration rate and cumulative infiltration increased with the burial depth of the porous membrane. This phenomenon may be attributed to the increased water potential gradient in the soil layer above the membrane, which intensifies with increasing burial depth, thereby enhancing the soil infiltration rate. These results were consistent with those reported by Ren et al.[45]. In addition, the soil infiltration rate and cumulative infiltration increased with increasing spacing between porous membranes. The underlying reason for this may be the dynamic changes in hydraulic gradients resulting from variations in the convergence time of the wetting fronts. When the spacing is minimal, the wetting fronts converge more quickly, leading to rapid saturation of the local water content in the convergence area. This significantly diminished the potential gradient of the soil matrix, resulting in a reduction in permeability. Conversely, a larger spacing delayed the convergence process of the wetting fronts, allowing the soil surrounding the membrane pores to sustain a higher hydraulic gradient for an extended period, thereby promoting prolonged water infiltration and increasing cumulative infiltration. Therefore, optimizing the structural parameters of porous membranes can effectively mitigate water infiltration, reduce deep leakage, and enhance water utilization efficiency.

4.3 Establishment and prospects of estimation model

In the fitting analysis of mathematical models, Liu et al.[46] examined the influence of interlayer soil on the moisture infiltration characteristics of heavily saline-alkaline soils. They found that the Kostiakov infiltration model could more accurately represent the moisture infiltration of interlayer soils with varying profile configurations, thereby providing a theoretical and scientific basis for the rational development and utilization of heavily saline-alkaline land in the future. Currently, there are no reported studies, either domestically or internationally, on estimation models for steady infiltration rates and cumulative infiltration using underground porous-membrane technology. Therefore, this study analyzed the changes in infiltration rates and cumulative infiltration of underground porous membranes under various influencing factors and found that irrigation duration and technical parameters had differing degrees of impact. Furthermore, this study developed an estimation model for steady infiltration rates and cumulative infiltration by incorporating the saturated hydraulic conductivity, film-laying parameters, and irrigation duration. The model is straightforward and exhibits high predictive accuracy, which can facilitate the determination of optimal parameters for underground porous membranes, allowing operators to conduct rapid on-site evaluations. Unfortunately, the interaction effects of film-laying parameters were not considered in the estimation model. Future work will need to incorporate the interactions among various

influencing factors to further optimize the model and enhance its accuracy.

The limitations of this study lie in the fact that underground porous membranes, an innovative technology for moisture regulation, are still in the exploratory phase. This study only investigated the effects of underground porous membrane diameter, spacing, and burial depth on soil infiltration characteristics. Future studies should systematically investigate the patterns of soil moisture evaporation, salt migration, and crop growth under various combinations of technical parameters related to underground porous membranes. In addition, the calculated values derived from the model established in this study demonstrated good consistency with the measured values. However, some discrepancies persist. These discrepancies may be attributed to the consideration of a limited number of influencing factors, which could have affected the accuracy of the results. Therefore, further research incorporating multiple factors is necessary to optimize the model, enhance its universality, and achieve theoretical advancements in underground porous-membrane technology.

5 Conclusions

Through a combined approach of numerical simulation and experimental validation, this study systematically investigated the effects of various influencing factors on the soil infiltration characteristics of underground porous membranes under four aeolian sandy soil conditions. An estimation model was developed of the soil steady infiltration rate and cumulative infiltration. The results indicated that the installation of underground porous membranes effectively reduced soil moisture infiltration capacity. Under the four aeolian sandy soil conditions, the initial infiltration rates for all treatments were relatively high, and no significant differences were observed. As infiltration progressed and reached the steady infiltration stage, the minimum reduction in infiltration rate for the different porous membrane treatments was 2.86 times lower compared to the CK treatment. Under various treatments with porous membranes, both the soil infiltration rate and cumulative infiltration increased with an increase in the saturated hydraulic conductivity, porous membrane diameter, burial depth, and spacing. A multiplicative power function model was developed to describe the relationship between the steady-state infiltration rate and several factors, including saturated hydraulic conductivity, porous membrane diameter, burial depth, and spacing, with a coefficient of determination of R^2>0.99. The power function exponents were 1.14, 1.04, 0.48, and 0.30, and the power function coefficient was 0.209. Experimental validation confirmed the reliability of the model, which exhibited an RMSE of 0.143 L/h and an NSE of 0.994. The established model serves as a valuable reference for selecting parameters for underground porous membrane irrigation technology. A cumulative infiltration estimation model for underground porous membranes was developed based on the Kostiakov infiltration model. This model incorporates factors such as saturated hydraulic conductivity, porous membrane diameter, burial depth, spacing, and irrigation duration. The reliability of the estimation model was assessed using experimental data, resulting in an RMSE of approximately 0.028 L and an NSE of approximately 0.999. The model demonstrated good predictive performance, and the proposed quantitative model can provide a scientific basis for technological optimization and widespread application.

Acknowledgements

This study was jointly supported by the National Natural Science Foundation of China (Grant No. 51969027), Corps Financial Science and Technology Plan Projects of Xinjiang Province, China (Grant No. 2021DB012, 2023AB059), and Ministry of Science and Technology of the People's Republic of China - Third Comprehensive Scientific Expedition to Xinjiang (Grant No. 2021xjkk0804).

[References]

[1] Guo B, Wei C X, Yu Y, Liu Y F, Li J L, Meng C, et al. The dominant influencing factors of desertification changes in the source region of Yellow River: Climate change or human activity? Sci Total Environ, 2022; 813: 152512.

[2] Zhi Y, Liu S L, Wang T, Duan H C, Kang W P. Quantifying the impact of natural and human activity factors on desertification in the Qinghai-Tibetan Plateau. Catena, 2024; 246: 108392.

[3] Chen S C, Chen X, Zuo H J, Yan M, Wang H B, Li X L. Soil compounding promotes the improvement of aeolian sandy soil in the Mu Us Sandy Land. Front Environ Sci, 2024; 12: 1435618.

[4] Qi F, Kunihiko E, Guodong C. Soil water and chemical characteristics of sandy soils and their significance to land reclamation. J Arid Environ, 2002; 51(1): 35–54.

[5] Ebrahimian H, Liaghat A, Parsinejad M, Abbasi F, Navabian M. Comparison of one-and two-dimensional models to simulate alternate and conventional furrow fertigation. J Irrig Drain Eng, 2012; 138(10): 929–938.

[6] Jiru M, Van Ranst E V. Increasing water productivity on Vertisols: implications for environmental sustainability. J Sci Food Agric, 2010; 90(13): 2276–2281.

[7] Bruckler L, Lafolie F, Ruy S, Granier J, Baudequin D. Modelling the agricultural and environmental consequences of non-uniform irrigation on a maize crop: 1. Water balance and yield. Agron, 2000; 20(6): 609–624.

[8] Rockström J, Jansson P E, Barron J. Seasonal rainfall partitioning under runon and runoff conditions on sandy soil in Niger: On-farm measurements and water balance modelling. J Hydrol, 1998; 210(1-4): 68–92.

[9] Muralidharan D, Knapp K C. Spatial dynamics of water management in irrigated agriculture. Water Resour Res, 2009; 45(5). doi: 10.1029/2007WR006756.

[10] Abbasi F, Adamsen F J, Hunsaker D J, Feyen J, Shouse P, Van Genuchten M T. Effects of flow depth on water flow and solute transport in furrow irrigation: Field data analysis. J Irrig Drain Eng, 2003; 129(4): 237–246.

[11] Zhao Y G, Pang H C, Wang J, Huo L, Li Y Y. Effects of straw mulch and buried straw on soil moisture and salinity in relation to sunflower growth and yield. Field Crops Res, 2014; 161: 16–25.

[12] Zhang Z Q, Wang Z J, Chen K Y, Wang S P, Ding Y P, Huang Y X, et al. Investigation on the lateral anti-seepage capacity of a vertical soil sand layer (VSSL) in a sunken lawn. J Hydro-environ Res, 2021; 38: 44–52.

[13] Zhou X L, Wang H, Chen Q G, Ren J Z. Coupling effects of depth of film-bottomed tillage and amount of irrigation and nitrogen fertilizer on spring wheat yield. Soil Tillage Res, 2007; 94(1): 251–261.

[14] Jin Z Q, Shah T, Zhang L, Liu H Y, Peng S B, Nie L X. Effect of straw returning on soil organic carbon in rice–wheat rotation system: A review. Food Energy Secur, 2020; 9(2): e200.

[15] Rong Y, Wang C, Hu Z Q. Effects of different layer positions of topsoil alternatives on infiltration and evaporation of sandy soil water. J Agric Resour Environ, 2022; 39(5): 967–977.

[16] Man D Q, Xu X Y, Wu C R, Yang Z H, Liu S Z. Research on seedling cultivation of pinus sylvestris at film-bottomed sand land in arid desert area. J Soil Water Conserv, 2003; 17(3): 170–173.

[17] Qin J H, Hong M, Yan C X, Aizimaitijiang Z E D, Wang C Y, Liu Y P. Effects of porous film mulching in root zone on water infiltration and evaporation of Hetian aeolian sandy soil. J Water Resour Water Eng, 2021; 32(2): 233–240.

[18] Hong M, Zhao J H, Mu H X, Ma Y J. Effects of porous film mulching in root zone on soil moisture. Agric Res Arid Areas, 2013; 31(4): 21–25. (in Chinese)

[19] Qin J H. Effect of porous film in root layer on water movement and the growth of malabar spinach in the aeolian sandy soil. Master dissertation. Xinjiang: Xinjiang Agricultural University, 2021; 3: 50p. (in Chinese) doi: 10.27431/d.cnki.gxnyu.2021.000187.

[20] Šimůnek J, Šejna M, Van Genuchten M T. New features of version 3 of the HYDRUS (2D/3D) computer software package. J Hydrol Hydromech,

2018; 66(2): 133–142.
[21] Šimůnek J, Van Genuchten M T, Šejna M. Recent developments and applications of the HYDRUS computer software packages. Vadose Zone J, 2016; 15(7): 1–25.
[22] Fan Y W, Shi J H, Shi W, Nie W B. Soil water infiltration characteristics for drip irrigation of seedlings to reduce aeolian erosion of sandy soils. J Irrig Drain Eng, 2024; 150(6): 04024033.
[23] Sun M, Mao X M, Chen J, Feng S Y. Laboratory experiment and simulation on canal seepage through sand interlayer. Transactions of the CSAE, 2010; 26(8): 33–38. (in Chinese)
[24] Van Genuchten M T. A closed-form equation for predicting the hydraulic conductivity of unsaturated soils. Soil Sci Soc Am J, 1980; 44(5): 892–898.
[25] Mualem Y. A new model for predicting the hydraulic conductivity of unsaturated porous media. Water Resour Res, 1976; 12(3): 513–522.
[26] Chen Y X, Gao G L, Zhang Y, Ding G D, Piao Q H, Zhao Y, et al. Characteristics of particle size distribution in aeolian sandy soil of hulunbuir sandy land. J Beijing Forest University, 2019; 41(8): 124–130. (in Chinese)
[27] Wei B M, Zhao X. Effect of addition of feldspathic sandstone on improvement of aeolian sand soil quality and the time effect. Res Soil Water Conserv, 2017; 24(6): 16–21. (in Chinese)
[28] Ma H X, Sun Q, Lu H T, Ma W L, Jiang P, Zhang X J, et al. Impact of initial soil water content on infiltration of irrigation water in aeolian sandy soil. J Irrig Drain Eng, 2023; 42(7): 52–59. (in Chinese)
[29] Dong Y Y, Hu S J, Zhao C Y, Zhu H, Wang D D, Ding Z Y. Determination of permeability coefficient of aeolian sandy soil in interdune areas at the southern edge of the Gurbantunggut desert using one-dimensional horizontal infiltration test. Arid Land Geogr, 2017; 40(4): 729–736. (in Chinese)
[30] Merrill S D, Tanaka D L, Hanson J D. Root length growth of eight crop species in Haplustoll soils. Soil Sci Soc Am J, 2002; 66(3): 913–923.
[31] Cai H G, Ma W, Zhang X Z, Ping J Q, Yan X G, Liu J Z, et al. Effect of subsoil tillage depth on nutrient accumulation, root distribution, and grain yield in spring maize. Crop J, 2014; 2(5): 297–307.
[32] Yang H S, Xu M M, Li Y F, Xu C X, Zhai S L, Liu J. The impacts of ditch-buried straw layers on the interface soil physicochemical and microbial properties in a rice-wheat rotation system. Soil Tillage Res, 2020; 202: 104656.
[33] Li B N, Shen L X, Liu S H. A comparison of soil water infiltration models of moistube irrigation. Ital J Agron, 2024; 19(1): 100001.
[34] Willmott C J. Some comments on the evaluation of model performance. Bull Am Meteorol Soc, 1982; 63(11): 1309–1313.
[35] Nash J E, Sutcliffe J V. River flow forecasting through conceptual models part I—A discussion of principles. J Hydrol, 1970; 10(3): 282–290.
[36] Zhang T W, Chen W, Chen X Y, Zhi R J, Chen L, Zhang H B, et al. Effects of typical soil and stratification thickness on water infiltration characteristics in central ningxia. Meteorol Environ Res, 2024; 15(4): 58–65. (in Chinese)
[37] Li Y, Ren X, Hill R, Malone R, Zhao Y. Characteristics of water infiltration in layered water-repellent soils. Pedosphere, 2018; 28(5): 775–792.
[38] Xu Q, Liu H G, Li M S, Li P F. The presence of the biochar interlayer effectively inhibits soil water evaporation and salt migration to the soil surface. Agric, 2023; 13(3): 638.
[39] Du Z D, Shao L T. Effects of film placed underground on deep percolation of planting soil for cultivating celery in greenhouses. South-to-North Water Transfer Water Sci Technol, 2013; 11(3): 160–164. (in Chinese)
[40] Cheng Q, Tang C S, Xu D, Zeng H, Shi B. Water infiltration in a cracked soil considering effect of drying-wetting cycles. J Hydrol, 2021; 593: 125640.
[41] Yao M Z, Li B, Wang T L, Feng X. Effects of straw size in buried straw layers on water movement in adjacent soil layers. Int J Agric & Biol Eng, 2016; 9(2): 74–84.
[42] Cao J S, Liu C M, Zhang W J, Guo Y L. Effect of integrating straw into agricultural soils on soil infiltration and evaporation. Water Sci Technol, 2012; 65(12): 2213–2218.
[43] Lipiec J, Kuś J, Słowinska-Jurkiewicz A, Nosalewicz A. Soil porosity and water infiltration as influenced by tillage methods. Soil Tillage Res, 2006; 89(2): 210–220.
[44] Fan Y W, Shi W, Shao X X, Zhang C Y, Yin W F. Infiltration reduction characteristics and a simplified calculation model of film hole irrigation during interference infiltration. Irrig Drain, 2022; 71(1): 35–47.
[45] Ren J, Wang H, Zhou X L, Chen D Q. Study on dynamic variation law of film-bottomed sandy soil moisture. J Gansu Agric Univ, 2000; 35(2): 152–156. (in Chinese)
[46] Liu H B, Wu B, Zhang J H, Bai Y G, Li X W, Zhang B. Influence of interlayer soil on the water infiltration characteristics of heavy saline-alkali soil in southern Xinjiang. Agron, 2023; 13(7): 1912.